

Hepatic bile acid synthesis and secretion: Comparison of *in vitro* methods

Véronique M.P. de Bruijn^{a,*}, Zhenguo Wang^{b,c}, Wouter Bakker^a, Weijia Zheng^a, Bart Spee^c, Hans Bouwmeester^a

^a Division of Toxicology, Wageningen University & Research, the Netherlands

^b Division of Pharmacology, Utrecht Institute for Pharmaceutical Sciences, Faculty of Science, Utrecht University, Utrecht, the Netherlands

^c Department of Clinical Sciences, Faculty of Veterinary Medicine, Utrecht University, Utrecht, the Netherlands

ARTICLE INFO

Keywords:

Bile acids and salts

Cholestasis

New approach methodologies

ABSTRACT

Reliable hepatic *in vitro* systems are crucial for the safety assessment of xenobiotics. Certain xenobiotics decrease the hepatic bile efflux, which can ultimately result in cholestasis. Preclinical animal models and the currently available *in vitro* systems poorly predict a xenobiotic's cholestatic potential. Here, we compared the phenotype and capacity of three liver derived *in vitro* systems to emulate human functionality to synthesize and secrete bile acids (BAs).

To this end, basal BA production of sandwich cultured human hepatocytes (SCHHs), HepaRG cells (HepaRGs) and hepatocyte-like intrahepatic cholangiocyte organoids (ICO-heps) were analysed, and the effect of the known BSEP (Bile Salt Export Pump)-inhibitors bosentan and lopinavir on BA disposition in SCHHs and HepaRGs was quantified. RT-qPCR of selected target genes involved in maturation status, synthesis, transport and conjugation of BAs was performed to mechanistically underpin the observed differences in BA homeostasis.

ICO-heps produced a (very) low amount of BAs. SCHHs are a powerful tool in cholestasis-testing due to their high basal BA production and high transporter expression compared to the other models tested. HepaRGs were responsive to both selected BSEP-inhibitors and produced a BA profile that is most similar to the human *in vivo* situation, making them a suitable and practical candidate for cholestasis-testing.

1. Introduction

Drug-induced liver injury (DILI) is one of the foremost reasons for drug-withdrawal, and has thus large financial consequences for the pharmaceutical industry (van Tonder et al., 2013). Drug-induced cholestasis is a subgroup of DILI and refers to impeded bile flow leading to the accumulation of bile acids (BAs) in the liver and subsequent spillage to the systemic circulation (Noor, 2015). Not only drugs, but also the phytotoxins like pyrrolizidine alkaloids, food additives, and biocides can cause cholestasis (Lu et al., 2021; Vilas-Boas et al., 2019, 2020). Causes of cholestasis range from changes in transporters to hepatocellular or bile canaliculi changes as described in an Adverse Outcome Pathway (AOP) (Gijbels et al., 2020). Currently, hepatic safety testing of drugs is performed predominantly by *in vivo* screening. However, animal studies can only predict 50 % of human drug induced liver injury, including cholestasis (Olson et al., 2000). Due to the poor predictivity as well as the ethical constraints of animal testing, new

approach methodologies (NAMs) to assess the cholestatic potential of xenobiotics are being developed (Deferm et al., 2019). Presently available *in vitro* models detect hardly half of the clinical DILI events (Laverty et al., 2010), hence research is ongoing to design *in vitro* models with higher predictivity. Next, the optimal *in vitro* model would be suitable for long-term culture and not require fresh liver tissue (Ramli et al., 2020; Vinken, 2018).

BAs are the major functional components of bile, and have been known to serve as emulsifiers of dietary lipids and lipid-soluble vitamins in the intestine for a long time. Additionally, BAs are increasingly recognized as important signaling molecules between the gut microbes and the host. BAs are synthesized in the liver via cytochrome P450 (CYP)-mediated oxidation of cholesterol. The classical pathway of BA synthesis is initiated by CYP7A1 and the alternative pathway is initiated by CYP27A1 (Axelson et al., 2000). Via various liver enzymatic reactions, ultimately the primary BAs cholic acid (CA) and chenodeoxycholic acid (CDCA) are formed in humans. In the liver, these primary

Abbreviations: AOP, Adverse Outcome Pathway; BA, bile acid; ICO-heps, hepatocyte-like intrahepatic cholangiocyte organoids; SCHH, sandwich-cultured human hepatocytes; DILI, drug-induced liver injury.

* Corresponding author.

E-mail address: veronique.debruijn@wur.nl (V.M.P. de Bruijn).

<https://doi.org/10.1016/j.toxlet.2022.06.004>

Received 15 March 2022; Received in revised form 30 May 2022; Accepted 9 June 2022

Available online 17 June 2022

0378-4274/© 2022 The Author(s). Published by Elsevier B.V. This is an open access article under the CC BY license (<http://creativecommons.org/licenses/by/4.0/>).

BAs are conjugated with taurine or glycine, resulting in tauro- or glycocholic acid (TCA, GCA) and tauro- or glycochenodeoxycholic acid (TCDCa, GCDCA). Subsequently, BAs are secreted from the liver into the bile canaliculus via the canalicular bile salt export pump (BSEP, ABCB11) (Jia et al., 2018). Inhibition of BSEP is a common cause of cholestasis, although inhibition does not necessarily lead to cholestasis and *vice versa* as cholestasis is not always linked with BSEP-inhibition (Gijbels et al., 2019). Recently, an AOP network was established for human hepatotoxicity (Arnesdotter et al., 2021), connecting 14 linear AOPs related to human hepatotoxicity. This network visualizes the complex interaction between biological processes involved in hepatotoxicity and elucidates multiple molecular initiating events (MIE), which rely on a sequence of key events (KEs) linked by key event relationships (KERs), that eventually could lead to hepatotoxicity, or cholestasis more specifically. In the current work, the effect of the known BSEP-inhibitors bosentan and lopinavir on the BA homeostasis was assessed in three different *in vitro* models. Bosentan inhibits BSEP in a non-competitive nature (Fattinger et al., 2001), while lopinavir leads to transcriptional repression of BSEP via interaction with farnesoid X receptor (FXR) (Garzel et al., 2014).

Upon secretion to the bile duct, BAs are transported to the intestine, where the gut microbes metabolize BAs to a wide array of primary and secondary BAs (Chiang, 2017; Jia et al., 2018). The BAs are reabsorbed into enterocytes and via the portal vein transported back to the liver. This cyclic process of BA secretion into the intestine, reabsorption and return to the liver is called enterohepatic recycling. Every day, around 90–95% of the intestinal BAs is recycled between the gut and the liver (Chiang, 2009; Dawson et al., 2009). Accordingly, a disturbance of the hepatic BA homeostasis will not only result in a local adverse effect on the liver, but will also distort the gut-liver axis.

Different cell-based systems emulate many liver functions involved in the development of drug-mediated hepatotoxicity and are therefore potential powerful *in vitro* models to study cholestasis. Various hepatic *in vitro* systems are available, ranging from simple monolayers to more advanced 3D cultures, using immortalized, primary, or stem cell derived cell sources. Culturing cells in a 3D spheroid configuration provides several benefits over monolayers, such as improved cell viability and phenotypic stability (Bell et al., 2018). Primary human hepatocytes cultured in a spheroid configuration maintain typical hepatocyte functions such as albumin and urea production and glycogen storage over a period of at least 5 weeks (Bell et al., 2016; Messner et al., 2018), and have shown promising for detecting DILI with a predictivity of 69 % (Vorrink et al., 2018).

In the current work we compare three different hepatic *in vitro* systems, *i.e.* sandwich cultured human hepatocytes (SCHHs), HepaRG cells in a monolayer configuration (HepaRGs) and hepatocyte-like intrahepatic cholangiocyte organoids in a 3D configuration (ICO-heps). Primary human hepatocytes are typically isolated from resected liver tissue with a two-step collagenase perfusion technique (Hengstler et al., 2000; LeCluyse and Alexandre, 2010). To overcome the limited availability of fresh liver tissue, cryopreserved hepatocytes are commercially available (Hengstler et al., 2000). Upon seeding, primary hepatocytes rapidly lose their typical *in vivo* morphology and differentiation status. When cultured in a sandwich configuration (sandwich cultured human hepatocytes, SCHH), *i.e.* between two layers of extracellular matrix, primary hepatocytes maintain their polarized phenotype for a longer period (Gijbels et al., 2019).

The hepatic hepatoma cell line HepaRG is another commonly used *in vitro* tool to study cholestasis. HepaRG cultures consist of two cell populations, one resembling hepatocytes and one resembling cholangiocytes (Kanebratt and Andersson, 2008). Next, organoid models could provide a solution for some of the drawbacks of primary

hepatocytes or hepatoma-derived cells. Here, we used intrahepatic cholangiocyte organoids (ICOs) isolated from human biopsies. These are bipotential cells able to differentiate towards the hepatic and cholangiocyte lineage (Marsee et al., 2021). ICOs can be differentiated towards hepatocyte-like cells (ICO-hep) when cultured in differentiation medium, which is deprived of inducers of proliferation such as Rspodin-1 and forskolin (Huch et al., 2015; Schneeberger et al., 2020; Verstegen et al., 2020).

The aim of the current work was to compare three hepatic *in vitro* systems for their ability to emulate human liver functionality to synthesize and secrete BAs. To this end, basal production of 18 BAs by SCHHs, HepaRGs and ICO-heps was measured using LC-MS/MS. qPCR of selected target genes involved in maturation status, BA synthesis, transport and conjugation was performed to mechanistically underpin the observed differences in BA homeostasis. We selected typical hepatocyte markers, *i.e.* albumin (*ALB*) and *CYP3A4*, to evaluate the hepatic lineage of the *in vitro* models (Marsee et al., 2021), and leucine-rich repeat-containing G-protein coupled receptor 5 (*LGR5*) as a stemness marker (Verstegen et al., 2020). The transporters selected were all part of the AOP for cholestasis, and *FXR* was included due to its central role in the regulation of BA homeostasis (Chiang and Ferrell, 2022; Gijbels et al., 2020). *CYP7A1* was selected as it is the rate limiting enzyme in the classical BA synthesis pathway, *CYP27A1* for its crucial role in the alternative BA synthesis pathway and bile acid coenzyme A:aminoacid N-acyltransferase enzyme (*BAAT*) to explain the differences observed in the conjugation state of the BAs produced by the SCHHs, HepaRGs and ICO-heps (Axelson et al., 2000; Chiang, 2013; Russell, 2003).

2. Materials and methods

2.1. Chemicals

Lopinavir (CAS 192725–17–0) and bosentan hydrate (CAS 157212–55–0) were purchased from Sigma-Aldrich (Zwijndrecht, the Netherlands). These compounds were dissolved in dimethyl sulfoxide (DMSO) (CAS 67–68–5). DMSO was purchased from Acros Organics (Geel, Belgium). For all cell cultures, we used HBSS, purchased from Gibco (Thermo Fisher Scientific, Paisley, UK) and trypsin-EDTA (trypsin 0.025 %/EDTA 0.01 %), purchased from Invitrogen (Thermo Fisher Scientific, Breda, the Netherlands).

2.2. Cell culture

Cryopreserved primary human hepatocytes (4 × lot HU8317 from one donor, 1 × lot HPP2380204 pooled from 5 donors), plating and cell maintenance supplement pack, FCS were purchased from Thermo Fisher Scientific (Landsmeer, the Netherlands). The plating and maintenance media were prepared in William's E culture medium (Thermo Fisher Scientific). Human hepatocyte thawing medium was obtained from Sigma-Aldrich. Lot HU8317 was obtained from a Caucasian 59-year old male, HPP2380204 contains hepatocytes from 4 females and 1 male, aged 52–69, all Caucasians. Primary human hepatocytes were thawed and plated according to the supplier's protocol. The seeding density was 400,000 cells per well in a 24-wells plate. The hepatocytes were allowed to form a monolayer for 6 h, and then the hepatocytes were overlaid with Matrigel (Corning, New York, NY, USA). The Matrigel was allowed to settle overnight. Hereafter, the cells were washed twice with HBSS and the medium was replaced with hepatocyte maintenance medium containing a solvent control, 50 μM bosentan or 50 μM lopinavir (final DMSO concentration, 0.5 % (v/v)). Previous research showed that 24 h exposure to 50 μM of bosentan and lopinavir did not reduce cell viability but decreased endogenous BA accumulation in HepaRGs and sandwich

cultured rat hepatocytes, respectively (Burbank et al., 2017; Griffin et al., 2013). 50 μ M bosentan did not result in cytotoxicity in sandwich cultured rat hepatocytes (Susukida et al., 2015). We performed a resazurin assay confirming that 24 h exposure to 50 μ M lopinavir did not affect HepaRG cell viability, see Appendix A for experimental details and results.

The HepaRG cell line was purchased from Biopredic International (Rennes, France). Passages 17–20 were used. The growth medium (GM) was composed of 500 mL William's E culture medium, completed with 5 mL penicillin-streptomycin solution (P/S) and 5 mL L-glutamine, all were purchased from Thermo Fisher Scientific, 0.25 mL 0.05 % human insulin (5 μ g/mL), 50 mL 10 % fetal calf serum (FCS) and 5 mL hydrocortisone-21-hemisuccinate (HCC) (10 mg/mL) were purchased from Sigma-Aldrich. The differentiation medium (DM) was composed of GM with 1.7 % (v/v) DMSO. Undifferentiated HepaRG cells were seeded at a density of 200,000 cells per well in a 6-wells plate and differentiated according to the supplier's protocol. Following the differentiation, medium was replaced by serum free medium, to deplete the cells from bovine BAs present in FCS. After 24 h, the cells were washed twice with HBSS and the medium was replaced with serum free medium containing a solvent control, 50 μ M bosentan or 50 μ M lopinavir (final DMSO concentration, 0.5 % (v/v)).

For the establishment of intrahepatic cholangiocytes organoids (ICOs), human liver biopsies were acquired from transplantation residual tissues that were used to ascertain if the liver tissue was healthy prior to transplantation at the Erasmus Medical Center Rotterdam approved by the Medical Ethical Council (MEC 2014–060). Establishment of ICO cultures was performed as follows: Liver biopsies were cut into small pieces and enzymatic dissociation was performed by incubation with type II collagenase (0.125 mg/mL; Gibco, Thermo Fisher Scientific, Waltham, MA, USA) and dispase (0.125 mg/mL; Gibco) in DMEM GlutaMAX (Gibco) containing 0.1 mg/mL DNase I (Roche, Basel, Switzerland), 1 % (v/v) FCS (Gibco) and 1 % (v/v) P/S (Gibco) at 37 °C in a water bath incubator. The supernatant of digested liver biopsies was collected and replaced with fresh enzyme-supplemented medium. Collection of supernatant and replacement with fresh medium was repeated three times. Single cells were collected and washed in cold DMEM GlutaMAX medium containing 1 % (v/v) FCS and 1 % (v/v) P/S and centrifuged at 400 g for 5 min. The single cells were mixed with cold Matrigel (Corning) and seeded in droplets (50 μ L) in a 24 well plate. After Matrigel gelation, expansion medium (EM) was added and cells were incubated at 37 °C with 5 % CO₂ (v/v). The expansion medium was Advanced DMEM/F12 medium (Gibco) supplemented with 1 % (v/v) HEPES (10 mM; Gibco), 1 % (v/v) P/S, 1 % (v/v) GlutaMax (Gibco), 10 % (v/v) Rspan-1 conditioned medium (the Rspan1-Fc-expressing cell line was a kind gift from Calvin J. Kuo), 2 % (v/v) B27 supplement without vitamin A (Invitrogen, Carlsbad, CA, USA), 1 % (v/v) N2 supplement (Invitrogen), Nicotinamide (10 mM; Sigma-Aldrich, St. Louis, MO, USA), N-acetylcysteine (1.25 mM; Sigma-Aldrich), fibroblast growth factor 10 (100 ng/mL; FGF10; Peprotech, Rocky Hill, NJ, USA), recombinant human (Leu15)-gastrin I (10 nM; GAS; Tocris Bioscience, Bristol, UK), 10 μ M forskolin (Tocris Bioscience), epidermal growth factor (50 ng/mL; EGF; Peprotech), hepatocyte growth factor (25 ng/mL; HGF; Peprotech) and A8301 (5 μ M; transforming growth factor b inhibitor; Tocris Bioscience). Organoids were passaged every 7–10 days at ratio of 1:3–1:4 and medium was refreshed every 2–3 days.

For the differentiation of ICOs to hepatocyte-like cells (ICO-heps), the BMP7 (25 ng/mL; Peprotech) was added in EM to prime differentiation for 3 days prior to shifting the cells to differentiation medium (DM). The DM was based on Advanced DMEM/F12 containing 1 % (v/v) HEPES, 1 % (v/v) P/S, 1 % (v/v) GlutaMAX, 2 % (v/v) B27 supplement without vitamin A, 1 % (v/v) N2 supplement, 1.25 mM N-acetylcysteine, 10 nM GAS, 50 ng/mL EGF, 25 ng/mL HGF, 500 nM A8301, fibroblast

growth factor 19 (100 ng/mL; FGF19; Peprotech), BMP-7 (25 ng/mL; Peprotech), dexamethasone (30 μ M; Sigma-Aldrich) and DAPT (10 μ M; Selleckchem, Houston, TX, USA). Organoids were kept in DM for 7 days and medium was refreshed every 2–3 days.

2.3. Time-dependent BA synthesis and secretion

Medium and cells were collected to quantify BA content in the different *in vitro* models at different time points. The cost-effectiveness of HepaRGs allowed us to test more different timepoints (0, 4, 24, 48 and 72 h) than was possible for the SCHHs or ICO-heps (0, 24, 48 h). No fresh medium was supplied between the time points in order to avoid a disturbance of the effect of BAs on their own synthesis and secretion. To sample the cells for subsequent analysis, trypsin was used to detach the cells from the plates. Firstly, cells were counted to be used for the normalization of the BA synthesis rate. Next, the cell suspensions were centrifuged for 5 min at 100 g at 4 °C, the supernatant was discarded and MilliQ was added to lyse the cells in order to measure intracellular BA content.

Cell and medium samples were kept for at least 15 min at 4 °C and subsequently transferred to – 80 °C. If all BA concentrations in the cell or medium samples were below the Limit of Detection (LOD), the samples were lyophilized in a Christ Alpha 1–2 LD plus freeze-dryer and redissolved in methanol. If BA concentrations were sufficiently high and no lyophilization was needed, the samples were mixed with ACN (50:50 v/v). Samples were centrifuged for 15 min at 15,000g and the supernatant was transferred to LC-MS/MS vials with inserts, and the BA content in the samples was analysed using LC-MS/MS.

For HepaRGs and SCHHs, triplicate measurements were performed in 3 independent experiments. For the SCHHs, we used 2 \times one donor and 1 \times 5 pooled donors. All 3 measurements were given the same weight in the data analysis, as we did not observe prominent interdonor differences based on the two batches of cells used in the analysis (Appendix Figure A. 2). For the ICO-heps duplicate measurements were performed for 4 different donors.

2.4. Bile acid profiling by LC-MS/MS

BA analysis was performed on a triple quadrupole LC-MS/MS system, model LCMS-8050 (Shimadzu Corporation, Japan), which was able to measure 18 BAs: UDCA, HDCA, CDCA, DCA, HCA, CA, GLCA, GDCA, GDCA, GCDCA, GCA, TUDCA, THDCA, TCDCA, TDCA, TCA, TLCA and LCA. BAs in samples and standards were separated on a Kinetex C18 column (1.7 μ m \times 100 A \times 50 mm \times 2.1 mm, Phenomenex 00B-4475-AN) using an ultra-high performance liquid chromatography (UHPLC) system (Shimadzu) with gradient elution using MilliQ water (0.01% formic acid) and methanol/acetonitrile (50 %v/50 %v) as mobile phase A and B, respectively. In order to enhance chromatographic performance, a C18 2.1 mm security guard (Phenomenex AJ0-8782) pre-column was used. Samples were injected (2 μ L) onto the column equilibrated in 30 % B at a flow rate of 0.4 mL/min. Initially, the mobile phase composition was 30% of B, followed by a linear ramp to 70 % of B until 10.0 min. A linear change to 98 % of B was executed until 11.0 min, which was held for another 7 min before returning to 30 % of B at 19.0 min and remained until 25 min. The column temperature was set at 40 °C and the sample tray temperature was set at 4 °C. The mass spectrometer (MS) used electrospray ionization (ESI) in negative ion mode. The ESI parameters were as below: Nebulizing gas flow, 3 L/minutes; drying gas flow and heating gas flow, 10 L/minutes; Interface temperature, 300 °C; Desolvation temperature, 526 °C; heat block temperature, 400 °C. Selective ion monitoring (SIM) and multiple reaction monitoring (MRM) were used for the detection of the BAs. The LOD was determined

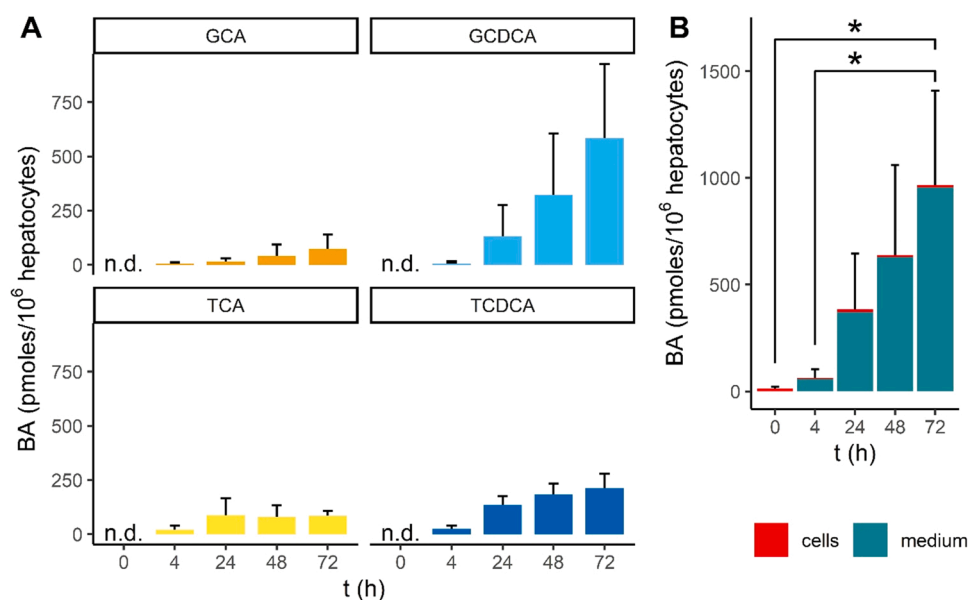


Fig. 1. Bile acid content upon incubation of differentiated HepaRG cells in serum-free cell culture medium between 0 and 72 h without medium renewal. A) Medium B) Intracellular and medium. Values represent the mean+SD of triplicate measurements in 3 independent experiments. Significance was assessed with a one way ANOVA followed by *post hoc* tests using Bonferroni's correction. Statistically significant altered bile acid contents are indicated with *. n.d. = not detected (< LOD). T/GCA=tauro/glycocholic acid, (T/G)CDCA=tauro/glycochenodeoxycholic acid.

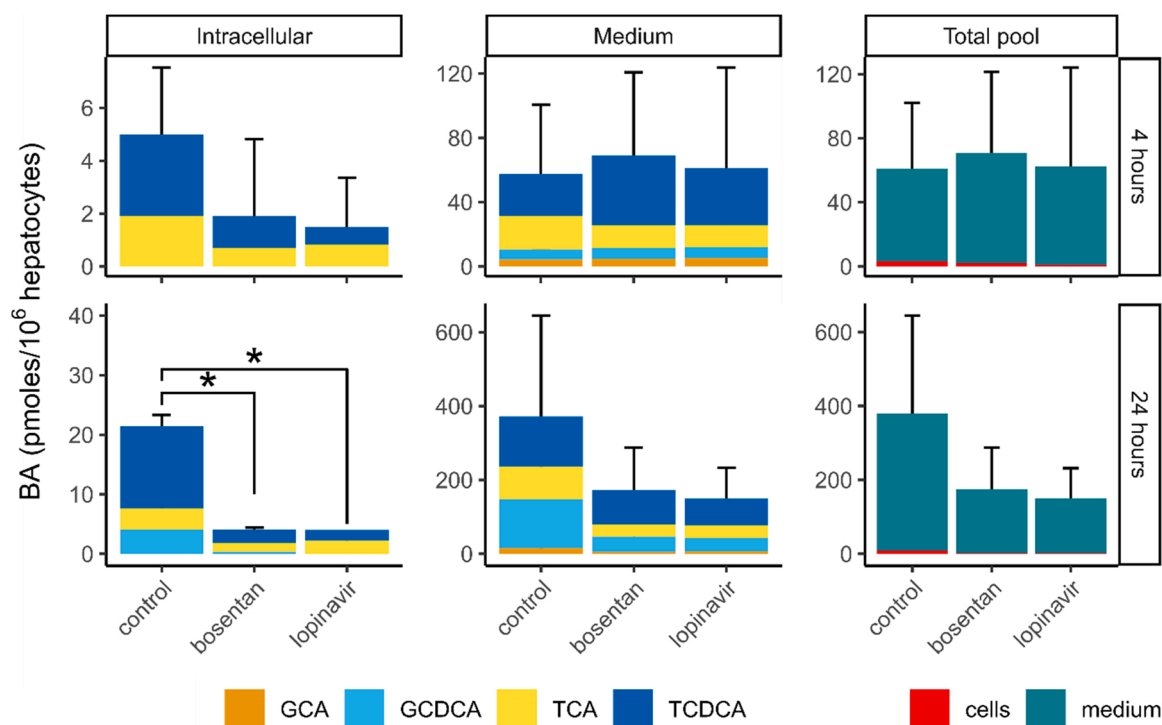


Fig. 2. Bile acid content of differentiated HepaRG cells incubated in serum-free cell culture medium upon incubation with a solvent control, 50 μM bosentan or 50 μM lopinavir for 4 or 24 h. Values represent the mean+SD of triplicate measurements in 3 independent experiments. Significance was assessed with a one way ANOVA followed by *post hoc* tests using Dunnett's correction. Statistically significant altered bile acid contents are indicated with *. T/GCA=tauro/glycocholic acid, T/GCDCA=tauro/glycochenodeoxycholic acid.

as the lowest measurable concentration with a signal-to-noise-ratio larger than 3; limit of quantification (LOQ) was set at the lowest measurable concentration with a signal-to-noise-ratio larger than 10. LODs and LOQs were determined in methanol. Any BA concentration

below the LOQ was set to 0 for further analysis. As we observed a matrix effect on the sensitivity of our analytical method, standards for the calibration curve were prepared in the same matrix as the samples. Data were collected and processed using the LabSolutions software

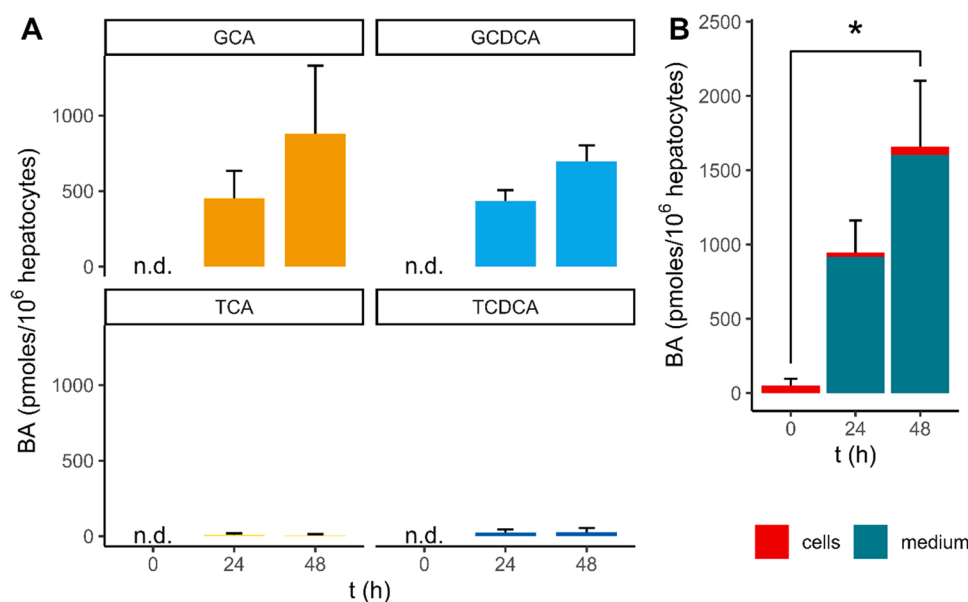


Fig. 3. Bile acid content upon incubation of sandwich cultured human hepatocytes in serum-free cell culture medium between 0 and 48 h without medium renewal. A) Medium B) Intracellular and medium. Values represent the mean+SD of triplicate measurements in 3 independent experiments. In total 6 different donors were assessed (2x one donor, 1x pooled 5 donors). Significance was assessed with a one way ANOVA followed by *post hoc* tests using Dunnett's correction. Statistically significant altered bile acid contents are indicated with *. T/GCA=tauro/glycocholic acid, T/GCDCA=tauro/glycochenodeoxycholic acid. n.d. = not detected (< LOD).

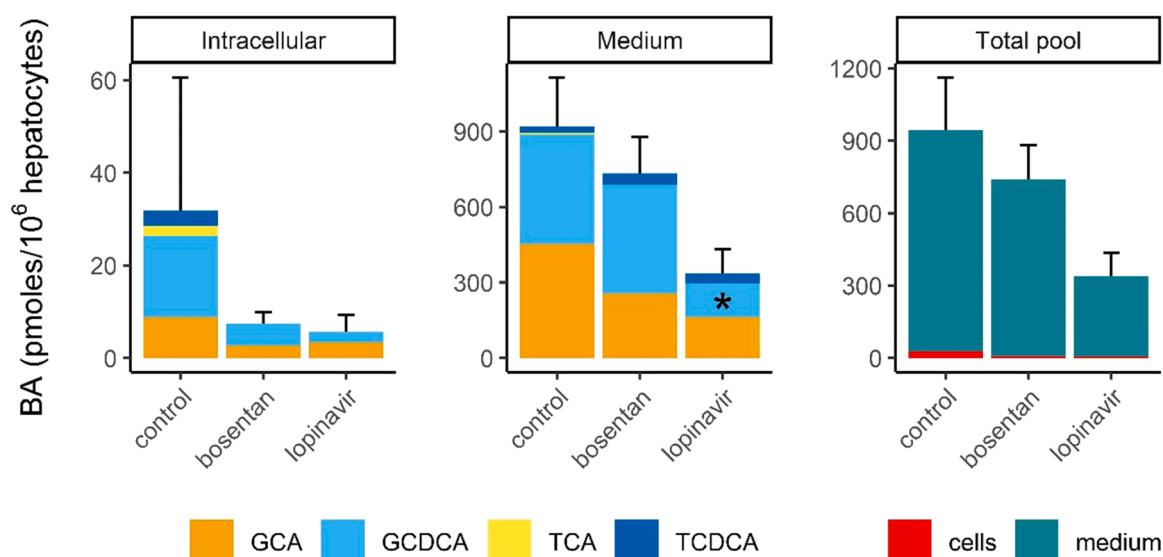


Fig. 4. Bile acid content of sandwich cultured human hepatocytes upon 24 h incubation with a solvent control, 50 μ M bosentan or 50 μ M lopinavir. Values represent the mean+SD of triplicate measurements in 3 independent experiments. In total 6 different donors were assessed (2 \times one donor, 1 \times pooled 5 donors). Significance was assessed with a one way ANOVA followed by *post hoc* tests using Dunnett's correction. Statistically significant altered bile acid contents are indicated with *. T/CA=tauro/glycocholic acid, T/GCDCA=tauro/glycochenodeoxycholic acid.

(Shimadzu). The MS parameters, LODs, LOQs and an exemplary chromatogram are provided [Appendix Table B.1](#) and [Fig. B.1](#).

2.5. RT-qPCR

RNA from HepaRGs, SCHHs and ICOs was isolated, in addition RNA was isolated from three liver biopsies from healthy tissues. The RNA

from the three liver biopsies was pooled and used as a reference. RNA from the HepaRGs and ICOs was isolated both after expansion and differentiation. HepaRG RNA was isolated after 14 days of maintenance in GM (HepaRG-GM), and after 14 days maintenance in GM followed by 14 days of differentiation in DM (HepaRG-DM). For the organoids, RNA was isolated after a period of growth in EM (ICOs), and after 7 days of differentiation in DM (ICO-heps). SCHHs RNA was isolated 30–32 h after

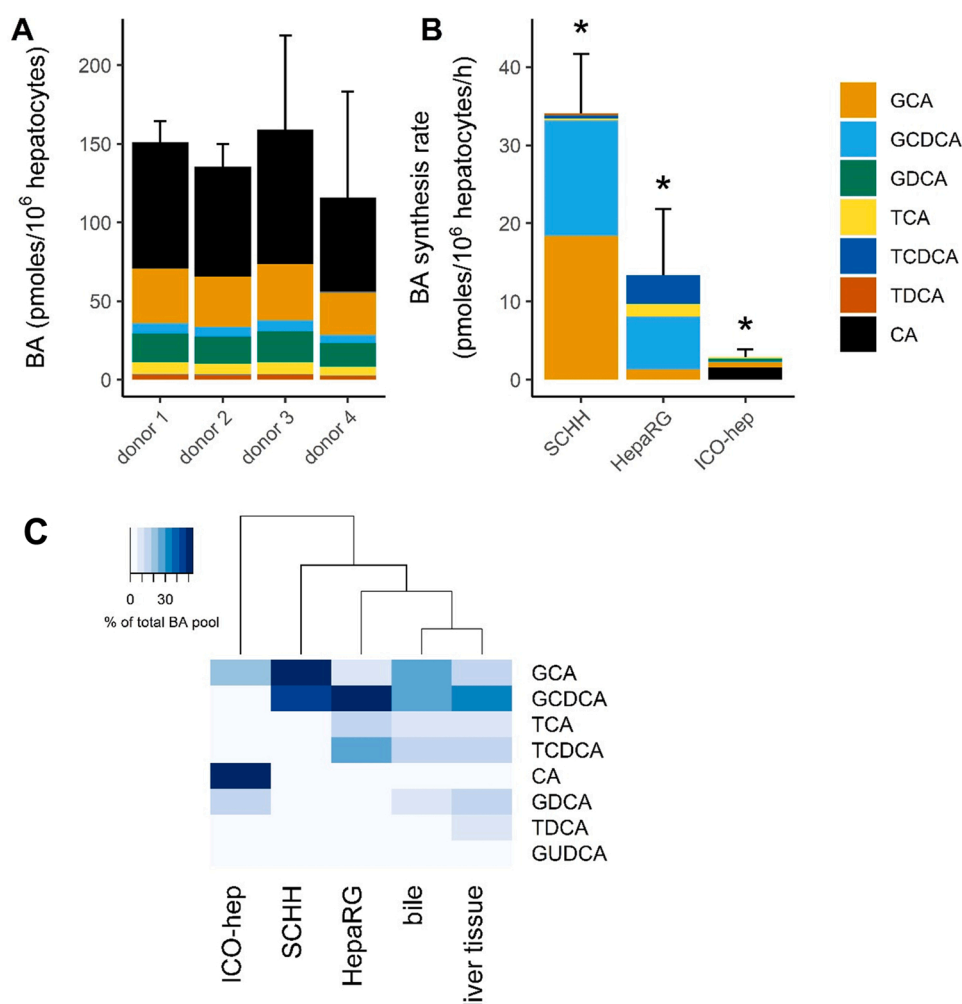


Fig. 5. A Bile acid secretion to serum-free cell culture medium by hepatocyte-like intrahepatic cholangiocyte organoids (ICO-hep) after 48 h without medium renewal. Values represent the mean+SD of duplicate measurements of 4 different donors. B) Comparison of bile acid synthesis rates of sandwich cultured human hepatocytes (SCHH), HepaRGs and ICO-heps. Data presented come from cells originating from 6, 1 and 4 different donors, respectively. Synthesis rates were corrected for intracellular bile acids present at $t = 0$ h, see Material & Methods. Significance was assessed with a one way ANOVA followed by *post hoc* tests using Bonferroni's correction. Statistically significant alterations are indicated with *. C) Hierarchical clustering analysis of bile acid profiles of ICO-heps, SCHH, HepaRG, bile or liver tissue. For the *in vitro* models (ICO-heps, SCHH, HepaRG) bile acid content was quantified in the medium. Bile acid content in bile and liver tissue were derived from literature, as reviewed by Rodrigues (2014). Bile acids were calculated as percentage of the entire pool in the respective tissue/fluid. Only bile acids that were > 1% of the total pool were included. (T/G)CA= (tauro/glyco)cholic acid, T/GCDCA=tauro/glycochenodeoxycholic acid, T/GDCA=tauro/glycodeoxycholic acid, GUDCA=glycourso-deoxycholic acid.

the Matrigel overlay. RNA was isolated using RNeasy Mini Kit (Qiagen; Hilden, Germany) following the manufacturer's instructions. cDNA synthesis was performed using the iScriptTM cDNA synthesis kit according to the manufacturer's instructions (Bio-Rad, Veenendaal, the Netherlands). RT-qPCR was used to measure the relative gene expression using validated primers (Table B.2) following the SYBR method (Bio-Rad). Normalization was done using the reference genes hypoxanthine-guanine phosphoribosyltransferase 1 (*HPRT1*), hydroxymethylbilane synthase (*HMBS*) and ribosomal protein L19 (*RPL19*). Lastly, relative mRNA levels were calculated and the levels in liver tissue were set to 1. For the organoids, samples from 5 donors were analysed, for HepaRG, 3 independent experiments were performed the cells originate from 1 donor, for SCHH we performed 4 independent experiments (1 donor HU8317).

2.6. Data analysis

The R package tidyverse version 1.3 was used for data exploration and visualization (Wickham, 2019). Statistical significance was determined by a one-way ANOVA with a Dunnett/Bonferroni correction for multiple tests. Results were considered statistically significant when p

< .05. Hierarchical clustering analysis was done in R using the heatmap.2 function from the R package gplots. Ward's clustering method with Euclidean as distance measure was used to compute the dendrograms. All analyses were performed in R version 4.0.2 (R Core Team, 2020).

For all *in vitro* models *de novo* BA synthesis rate was calculated as $(BA_{medium,t48} + BA_{cells,t48} - BA_{medium,t0} - BA_{cells,t0})/48$. BA synthesis rate was expressed in pmoles/10⁶ hepatocytes/h. For the HepaRGs, it was assumed that 50% of the cell population consisted of hepatocytes and 50 % of cholangiocytes (Cerec et al., 2007).

As a reference, the daily BA synthesis rate of a human liver was calculated based on a synthesis rate of 0.35 mg/g liver/day (Ellis et al., 1998), a hepatocellularity of 139×10^6 hepatocytes/g liver (Sohlenius-Sternbeck, 2006) and 1500 g of liver (Barter et al., 2007). This corresponds to about 240 pmoles/10⁶ hepatocytes/h.

3. Results

3.1. HepaRG cells secrete conjugated primary bile acids

HepaRGs secreted the conjugated primary BAs GCA, TCA, GCDCA

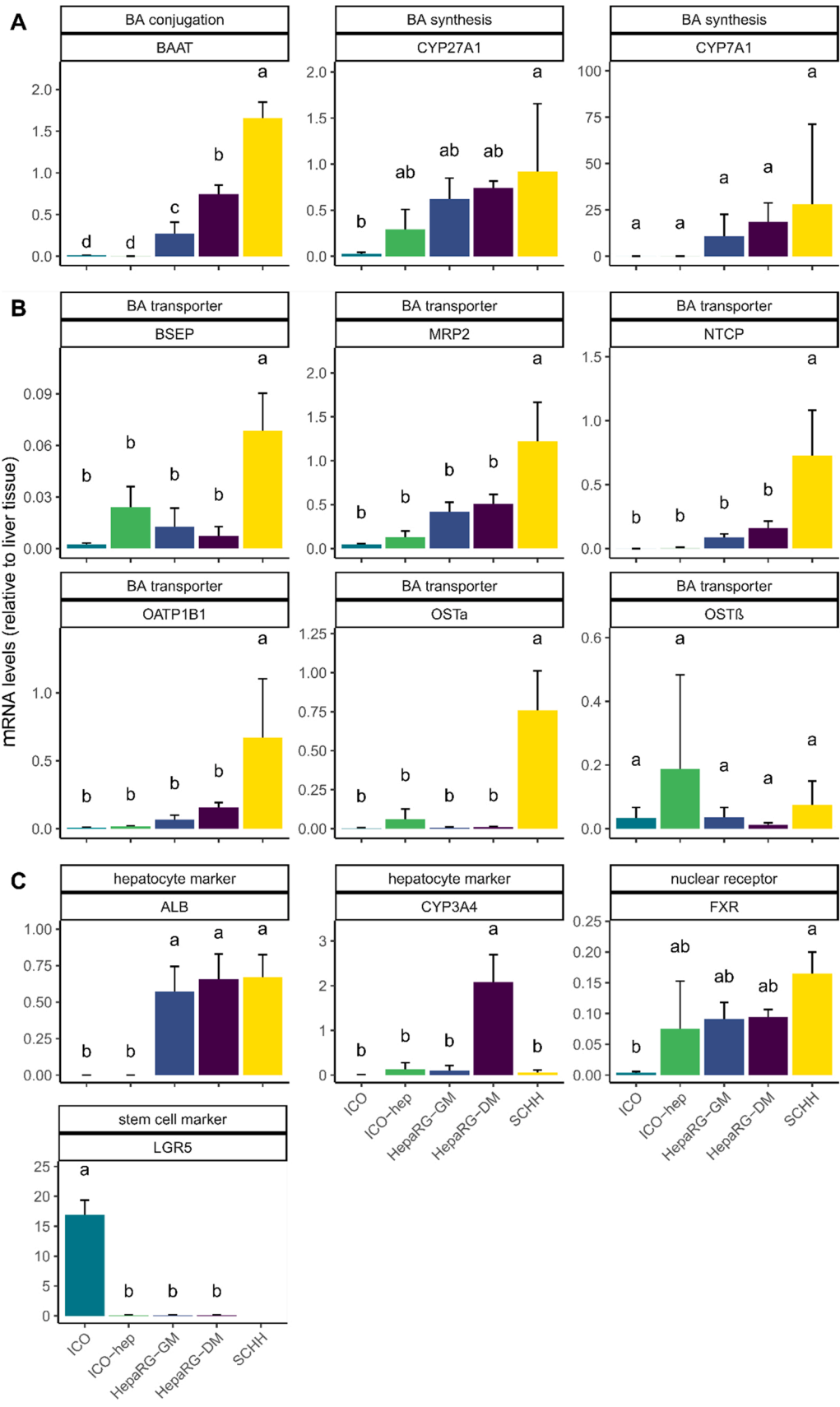


Fig. 6. mRNA levels of target genes in organoids under expansion or differentiation conditions (ICO, ICO-hep), HepaRGs under growth or differentiation conditions (HepaRG-GM, HepaRG-DM) and sandwich cultured human hepatocytes (SCHH). mRNA levels in a pooled liver biopsy sample were set to 1 (n = 1) as a reference. Data represent mean+SD. Organoids: 5 donors, HepaRG: 3 independent experiments, SCHH: 4 independent experiments, donor HU8317. For details about the target genes, see Table B.1. Groups that share the same letter (a or b) are not statistically significantly different. Significance was assessed with a one way ANOVA followed by *post hoc* tests using Bonferroni correction. A) enzymes involved in BA synthesis and conjugation, B) BA transporters, C) stem cell/hepatocyte markers.

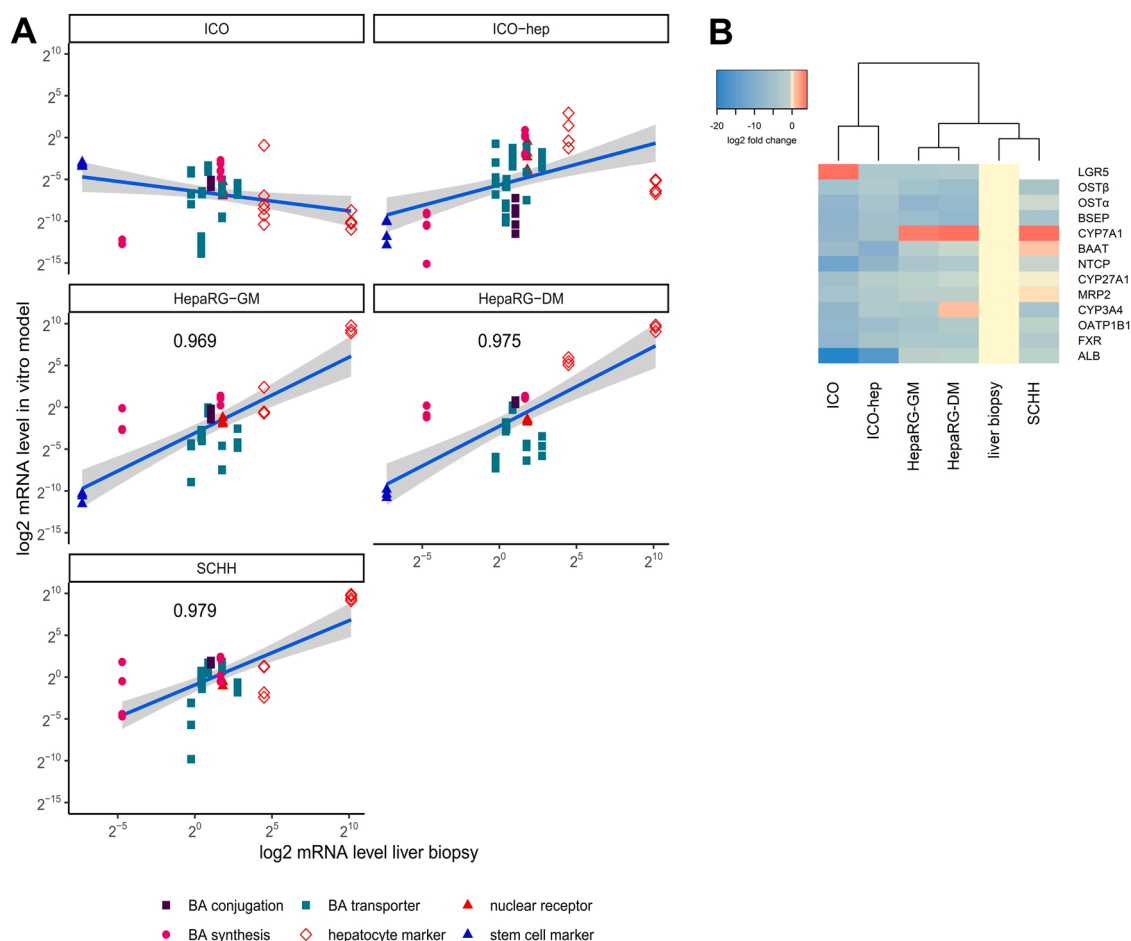


Fig. 7. Correlation of mRNA levels of selected target genes between organoids under expansion or differentiation conditions (ICO, ICO-hep), HepaRGs under growth or differentiation conditions (HepaRG-GM, HepaRG-DM) and sandwich cultured human hepatocytes (SCHH). Organoids: 5 donors, HepaRG: 3 independent experiments, SCHH: 4 independent experiments, donor HU8317. For details about the target genes, see [Appendix Table B.2](#)) Linear correlation between the *in vitro* models and liver biopsy. Pearson's correlation coefficient was calculated and shown in the plot if significantly different from 0. B) Hierarchical clustering analysis. Values were normalized to a pooled liver biopsy sample. Missing values are coloured white.

Table 1

Practical considerations and applicability domain of explored *in vitro* models.

	Cell type of origin	Intended cell type (s) after differentiation	Pros	Cons
HepaRG cells	Hepatocellular carcinoma	Hepatocytes and cholangiocytes (~ 50/50)	<ul style="list-style-type: none"> • Easy <i>in vitro</i> proliferation, maintenance and storage • Suitable for long term exposure • Reproducible • Robust 	<ul style="list-style-type: none"> • Tumorigenic phenotype
Hepatocyte-like intrahepatic cholangiocyte organoids (ICO-hep)	Intrahepatic cholangiocyte	Hepatocytes	<ul style="list-style-type: none"> • Unlimited availability and indefinite proliferation • Allows to study differences between donors 	<ul style="list-style-type: none"> • Low isolation and purification rate
Sandwich cultured human hepatocytes (SCHH)	Hepatocyte	–	<ul style="list-style-type: none"> • Golden standard • Allows to study differences between donors 	<ul style="list-style-type: none"> • Donor material needed for every experiment

and TCDCA ([Fig. 1A](#)). The concentrations of the remaining 14 BAs were below the LOQ (See Annex Table B.1 for the LOQs of all individual BAs). CDCA conjugates were more abundantly secreted than CA conjugates, with GCDCA being the most abundant BA in the cell culture medium. No unconjugated or secondary BAs were detected in the cells or medium. The amount of intracellular BAs did not change significantly over time, while the total BA pool (cells with medium) significantly increased after

72 h indicating *de novo* BA synthesis ([Fig. 1B](#)).

Upon 4 h or 24 h treatment with 50 μ M lopinavir or 50 μ M bosentan, no statistically significant alterations were observed in the medium or total BA pool, although a slight but not significant decrease in the medium BA content was observed after 24 h of treatment. The total intracellular BA content, as well as intracellular GCDCA and TCDCA specifically, decreased significantly upon 24 h treatment with bosentan

or lopinavir compared to the control (Fig. 2). After both 4 h and 24 h treatment with lopinavir, but not in the control or bosentan-treated cells, a small amount of CDCA was detected in both cells and the medium, however, the respective amount could not be quantified (below LOQ, data not shown).

3.2. SCHHs secrete mainly glycine conjugated primary bile acids

Sandwich cultured human hepatocytes (SCHHs) secreted all four conjugated primary BAs known to be present in humans. Glycine-conjugates were secreted more abundantly to the medium than taurine-conjugates, with GCA being the most abundant BA in the medium (Fig. 3A). Intracellular BAs did not change over time, but the total BA pool significantly increased after 48 h compared to $t = 0$ h (Fig. 3B).

The bosentan or lopinavir treatment did not induce any significant changes in the total or intracellular BA pool, however, the GCDCA content in the medium was significantly decreased upon lopinavir treatment and TCDCA was detected in the cells in the control, but not after lopinavir or bosentan treatment (Fig. 4). Small amounts of GDCA, TDCA and TCA were detected in the medium after bosentan and lopinavir treatment, however, these amounts could not be quantified (<LOQ, data not shown). TDCA and GDCA were not detected in the control medium (<LOD, data not shown).

3.3. ICO-heps produce a limited amount of bile acids

ICO-heps synthesized and secreted (very) low amounts of BAs. Up until 48 h after medium renewal, all BAs in the medium of ICO-heps were below the LOD (data not shown). After 48 h of incubation, CA and GCA comprised the majority of the secreted BAs. Four different liver biopsy donors were tested, and this resulted in similar BA secretion profiles after 48 h (no statistical differences in the levels of individual BAs between the different donors), see Fig. 5A. Therefore, the results from these different donors were averaged and compared with the other hepatic *in vitro* systems. Intracellular BA content was below the LOD at all of the tested time points (data not shown).

3.4. Comparison of bile acid profiles and synthesis rates

The *de novo* synthesis rate was the highest in SCHHs, followed by HepaRGs and lastly ICO-heps (Fig. 5B). As the BA levels produced by ICO-heps were so low, bosentan's and lopinavir's effect on the BA pool were not assessed. Next, the BA profile secreted by the different hepatic *in vitro* systems were visualized and compared with human *in vivo* BA profiles in liver tissue and bile using hierarchical clustering analysis (HCA) (Fig. 5C). The human *in vivo* data were obtained from literature (Rodrigues et al., 2014). The HCA revealed a large similarity between the BA profile in bile and liver tissue *in vivo*. The HepaRGs clustered more closely with the *in vivo* bile and liver data than SCHHs and ICO-heps.

3.5. Expression of BA transporters is the highest in SCHHs

Differential gene expression of the non-treated *in vitro* models was analyzed by RT-qPCR of samples from organoids, HepaRG and SCHHs. Organoids and HepaRG were analyzed under expansion/growth conditions (ICOs, HepaRG-GM) and differentiation conditions (ICO-heps, HepaRG-DM). The analysis revealed many differences in mRNA levels between the cell types. mRNA levels of enzymes responsible for BA synthesis (*CYP7A1* and *CYP27A1*) were comparable across ICO-heps, HepaRGs and SCHHs. Bile acid-CoA:amino acid N-acyltransferase (*BAAT*) mRNA levels were the highest in SCHHs followed by HepaRGs. ICOs and ICO-heps showed the lowest *BAAT* mRNA levels of the models

studied (Fig. 6A).

Interestingly, mRNA levels of most BA transporters were significantly higher in the SCHHs than in the differentiated HepaRGs and ICO-heps, *i.e.* mRNA levels of ATP-binding cassette, sub-family B member 11 (*ABCB11*, Bile Salt Export Pump (BSEP)), ATP binding cassette sub-family C member 2 (*ABCC2*, multidrug resistance-associated protein 2 (MRP2)), solute carrier family 10 member 1 (*SLC10A1*, Na^+ -taurocholate cotransporting polypeptide (NTCP)), solute carrier organic anion transporter family member 1B1 (*SLCO1B1*, organic anion transporting polypeptide 1B1 (OATP1B1)) and solute carrier family 51 subunit alpha (*SLC51A*, organic solute transporter α (OST α), but not its subunit OST β (*SLC51B*) (Fig. 6B). Stemness of the ICOs before differentiation was indicated by the presence of *LGR5*. Hepatic markers *ALB* and *CYP3A4* were slightly increased after differentiation (ICO-hep), indicating differentiation towards the hepatocyte lineage (Fig. 6C).

3.6. The mRNA profiles of SCHHs and HepaRGs are the most similar to a liver biopsy

HepaRG and SCHH mRNA levels show a strong correlation with those obtained for a liver biopsy (Pearson's $r > 0.96$), while there was no statistically significant correlation found between the mRNA levels of the selected target genes in ICOs/ICO-heps and the liver biopsy (Fig. 7A). HCA shows that SCHHs cluster the closest with the liver biopsy, followed by HepaRG-GM/HepaRG-DM, and in line with the correlation analysis, the ICOs/ICO-heps mRNA levels are the most distinctive from the liver biopsy (Fig. 7B).

4. Discussion

The current study compares the capacity of three different hepatic *in vitro* systems to emulate human liver functionality to synthesize and secrete BAs. BA synthesis rates and profiles, responsiveness to selected BSEP-inhibitors and selected target genes were analysed for: hepatocyte-like intrahepatic cholangiocyte organoids (ICO-heps), sandwich cultured human hepatocytes (SCHH) and HepaRG cells (HepaRGs). The data reveal that differentiated HepaRGs and SCHHs correlate the closest to human liver *in vivo* data at the selected endpoints.

In the current study, we employed organoids derived from biopsies of healthy human liver, and uniquely studied the BA synthesis and secretion capacity. Intrahepatic cholangiocyte organoids were isolated from liver biopsies and differentiated towards hepatocyte-like cells (ICO-heps) (Huch et al., 2015; Schneeberger et al., 2020). An advantage of tissue derived organoids, compared to induced pluripotent stem cells (iPSCs), is that they display high levels of genetic stability and are devoted to their tissue of origin (Prior et al., 2019). As the liver consists of multiple cell types, we evaluated the hepatocyte fate and maturation of the ICO-heps by assessing mRNA levels of stem cell and hepatocyte markers. Significant downregulation of the stem cell marker *LGR5* and increased hepatocyte markers upon differentiation suggests that the ICO-heps were differentiated towards the hepatic lineage. Typical liver functionalities, such as BA synthesis, glycogen storage, phase I and phase II drug metabolism and ammonia detoxification, have previously been identified in ICO-heps (Huch et al., 2015). However, single cell analysis of the human liver revealed a large diversity in cell (sub)types in the biliary tract, including cholangiocytes that express hepatocyte markers, such as *ALB*, *SERPINA1* and *CYP3A4* (Aizarani et al., 2019). Hence, it remains to be determined whether the ICO-heps used in the current study had truly differentiated towards a hepatocyte-phenotype, or whether they were cholangiocytes that upregulated some hepatocyte markers and perform BA synthesis.

A major advantage of ICO-heps over HepaRGs is their non-cancerous nature, and ICO-heps require drastically less fresh liver tissue than

SCHHs because of their indefinite proliferation capacity *in vitro* (Table 1). Currently, ICOs are explored to be used for mechanistic disease modeling (Nguyen et al., 2021), personalized medicine and drug screening (Broutier et al., 2017), and tissue transplantation (Huch et al., 2015; Reza et al., 2021).

From the three hepatic *in vitro* models tested, the *de novo* BA synthesis rate was the highest in SCHHs (31 ± 7 pmoles/ 10^6 hepatocytes/h), which is higher than the range reported in literature (7–19 pmoles/ 10^6 hepatocytes/h (Ellis et al., 1998; Sharanek et al., 2015)), but still 7-fold lower than the *in vivo de novo* synthesis rate by the human liver (Ellis et al., 1998; Sohlenius-Sternbeck, 2006). The BA *de novo* synthesis rate and BA profile produced by HepaRGs are consistent with literature (Sharanek et al., 2015). Both HepaRGs and SCHHs secrete, in line with previous reported data, conjugated primary BAs (Behr et al., 2020; Ellis et al., 1998; Sharanek et al., 2015). The most striking difference between the HepaRGs and SCHHs is the predominance of glycine-conjugated BAs secreted by SCHHs (96%), whereas HepaRGs also secrete a substantial amount of tauro-conjugates (42%). This discrepancy between these two models has been previously attributed to the tumour origin of HepaRGs (Sharanek et al., 2015). Compared to the *in vivo* situation the formation of tauro-conjugates by HepaRGs results in a BA profile more similar to the profile in liver and bile than the SCHHs, given that ~30% of BAs in human bile are tauro-conjugates (Rodrigues et al., 2014). The conjugation state of a BA depends on the substrate availability (glycine or L-cysteine, taurine's precursor) (Starokozhko et al., 2017). HepaRGs and SCHHs were both cultivated in William's E medium, hence differences in substrate availability cannot explain this differences in BA composition. The ICO-heps showed the lowest BA synthesis rate and the most distinct BA profile compared to human bile and liver tissue profiles. mRNA levels of *CYP7A1*, the rate limiting enzyme in BA synthesis, were comparable across all three *in vitro* models, but the *BAAT* mRNA levels were significantly lower in the ICO-heps. This provides a plausible explanation for the incomplete BA conjugation by ICO-heps and the subsequent abundance of CA. We found high *CYP3A4* levels and similar *ALB* and *FXR* levels in HepaRGs compared to SCHHs. Similar results were reported in literature for HepaRGs compared to primary human hepatocytes cultured in suspension (Kanebratt and Andersson, 2008). *CYP3A4* and *BSEP* mRNA levels were low in SCHHs compared to the pooled liver sample (fold change <0.1). A recent study showed that mRNA levels of a number of key hepatocyte genes, including *CYP3A4* and *BSEP*, were drastically reduced in SCHHs on day 2 of culture due to dedifferentiation. The SCHHs can redifferentiate after prolonged culturing (Yang and Li, 2021). Our analysis was performed on day 1, but dedifferentiation provides a plausible explanation for the low *CYP3A4* and *BSEP* RNA levels in the SCHHs compared to the pooled liver sample. mRNA levels of *ALB*, *CYP7A1* and *CYP27A1*, *BAAT* and the remaining BA transporters, except *OSTβ*, had a fold expression of > 0.5 compared to the pooled liver sample, indicating that the SCHHs had not fully dedifferentiated. Even though *BSEP* mRNA levels were low in SCHHs, we found that mRNA levels of all selected BA transporters, but not *OSTβ*, were significantly lower in HepaRGs than in SCHHs, which is in line with previous results (Susukida, Sekine et al., 2016). Irrespective of the low mRNA levels it has been shown that both HepaRGs and SCHHs have functional BA transporters and are suitable for BA transport studies (Bachour-El Azzi, Sharanek et al., 2015; De Bruyn et al., 2013; Guguene-Guillouzo and Guillouzo, 2019; Sharanek et al., 2015).

We next studied the responsiveness of the cell systems to a FXR-mediated transcriptional repression of BSEP by lopinavir (Garzel et al., 2014) and direct BSEP inhibition by bosentan (Fattinger et al., 2001) on the BA content in medium and cells. Bosentan exposure did not affect the amount of BAs secreted to the medium by HepaRGs, but resulted in a decrease of intracellular BA content in HepaRGs, confirming previous results (Burbank et al., 2017). The results point towards the presence of a compensatory mechanism to counteract or prevent intrahepatic BA accumulation. This adaptive response is visualized and described in the AOP for cholestasis, and indicates that through activation of the nuclear

receptors Farnesoid X receptor (FXR), Pregnane X receptor (PXR) and constitutive androstane receptor (CAR), sinusoidal BA efflux is increased by the upregulation of several ABC-transporters, such as *ABBC3* (MRP3) and *ABCC2* (MRP2), and hepatic BA influx is reduced by a down-regulation of *SLC10A1* (NTCP). These mechanisms have been verified for HepaRGs treated with bosentan using qPCR for various BA transporters and immunolabeling of MRP3 (Burbank et al., 2017). Lopinavir treatment resulted in similar changes in BA disposition in HepaRGs as bosentan. Lopinavir's agonistic effect on FXR-activation is expected to repress not only BSEP transcription, but also increase the sinusoidal BA efflux and reduce BA uptake. The observed similar alterations in the BA pool upon exposure of HepaRGs to lopinavir and bosentan, i.e. an intracellular BA reduction but no effects on BA secretion to the medium, suggest an at least partially shared mechanism of action between lopinavir and bosentan treatment. In the SCHHs, we have found a decrease in GCDCA medium content upon lopinavir-treatment, which was also found in a study with primary rat hepatocytes (Griffin et al., 2013). Previously, a decrease in GCA and GCDCA content in the cell lysate, and a decrease GCA in the culture medium, have been reported upon 24 h bosentan-treatment with concentrations ranging from 10 to 100 μ M in SCHHs (Lepist et al., 2014; Oorts, Van Brantegem et al., 2021), but we could not confirm this. No adverse effect of 24 h treatment with 50 μ M bosentan (Burbank et al., 2017) or lopinavir on HepaRG cell viability was observed (current study). An 192 h (8 day) exposure to 50 μ M bosentan reduced the viability of spheroid cultures primary human hepatocytes (Hendriks et al., 2016), while 24 h exposure to 50 μ M lopinavir or bosentan did not affect the cell viability of sandwich-cultured primary rat hepatocytes (Griffin et al., 2013; Susukida et al., 2015). Therefore, a reduction of cell viability of the human SCHHs following bosentan or lopinavir treatment cannot be fully excluded as a possible explanation for the observed differences in BA disposition in the SCHHs. As ICO-heps showed a low BA production, the applicability of this model to predict the effects of reduced BSEP activity was not assessed.

Collectively, the data reveal important differences in phenotype and BA homeostasis between the three human hepatic *in vitro* systems tested. The BA synthesis rate of SCHHs and HepaRGs is (still) superior to ICO-heps, and also their BA profiles and the mRNA levels of the selected target genes cluster closer together with the human *in vivo* situation than the ICO-heps. While SCHHs have the highest BA synthesis rate and BA transporter expression from the models tested, HepaRGs showed the most *in vivo* like BA profile and responsiveness to the selected BSEP-inhibitory or repressing compounds. By that, HepaRGs provide a powerful and practical *in vitro* model for cholestasis testing.

Funding information

Z. Wang and W. Zheng were supported by a scholarship for PhD candidates from the China Scholarship Council (No. 201808620130, No. 202003250128).

The authors declare no conflict of interest.

Declaration of Competing Interest

The authors declare the following financial interests/personal relationships which may be considered as potential competing interests. Weijia Zheng reports financial support was provided by China Scholarship Council. Zhenguo Wang reports financial support was provided by China Scholarship Council.

Acknowledgements

We would like to thank prof.dr.ir. I.M.C.M Rietjens for carefully proof-reading the manuscript. We thank L.H.J. de Haan for her skillful assistance in setting up the cell cultures.

Appendix A

See Figs. A.1–A.3.

Cell viability

The effect of lopinavir on the cell viability of the HepaRG cells was determined via the Resazurin assay. Resazurin sodium salt (CAS

62758–13–8) was purchased from Merck (Darmstadt, Germany). 560 μ M resazurin was dissolved in PBS, sterilized and stored in the dark at 4 °C. 96 wells plates with fully differentiated HepaRGs were exposed to 0–150 μ M lopinavir for 24 h. Next, 10 % v/v resazurin was added to the HepaRG cells. The plates were incubated at 37 °C for 4 h, protected from direct light. Fluorescence was measured using the SpectraMax® iD3 from Molecular Devices. The excitation wavelength was set on 560 nm and the emission wavelength on 590 nm.

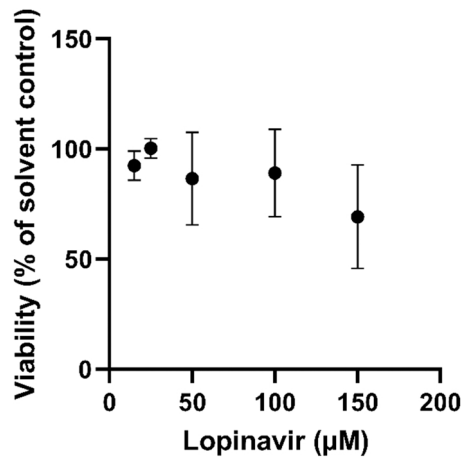


Fig. A. 1. Cell viability of HepaRGs upon 24 h treatment with different concentrations of lopinavir assessed using the resazurin assay. Values represent the mean \pm SD of triplicate measurements in 3 independent experiments.

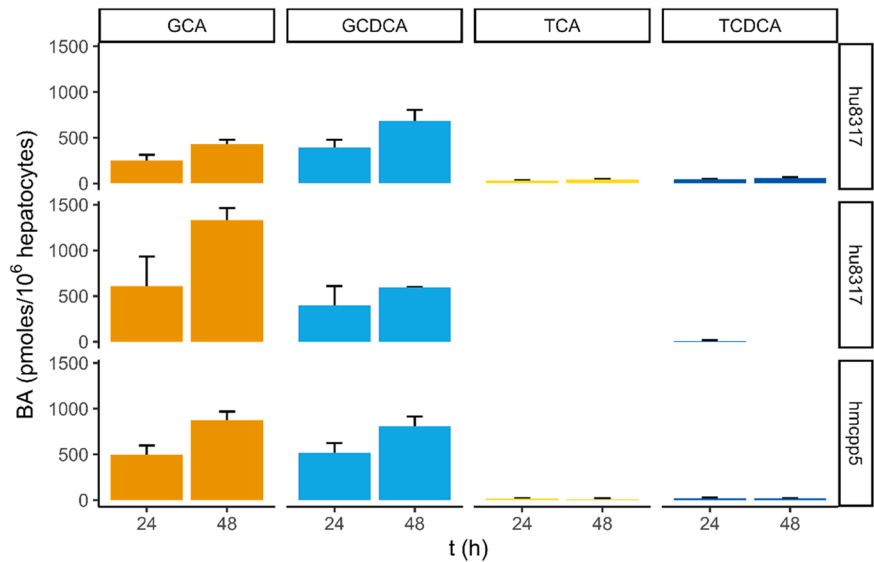


Fig. A. 2. Bile acid content upon incubation of sandwich cultured human hepatocytes in serum-free cell culture medium between 0 and 48 h without medium renewal. Each row represents the mean+sd of one biological replicate, measured in triplicate.

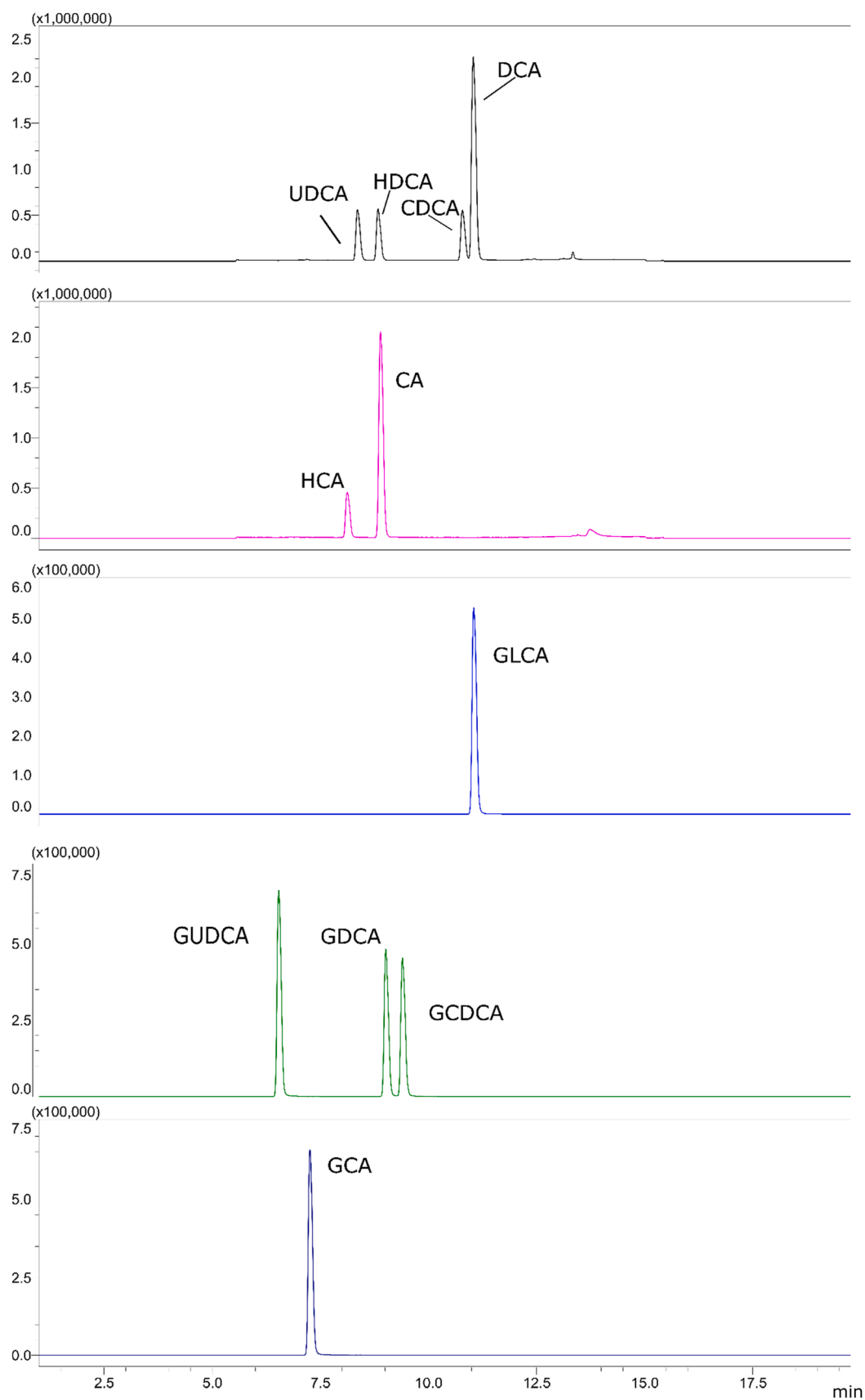


Fig. A.3. Chromatograms of LC-MS/MS run. 1 μ M of a mixture of 18 BAs in MeOH. Abbreviations, MS parameters and LOD are presented in [Table B.1](#).

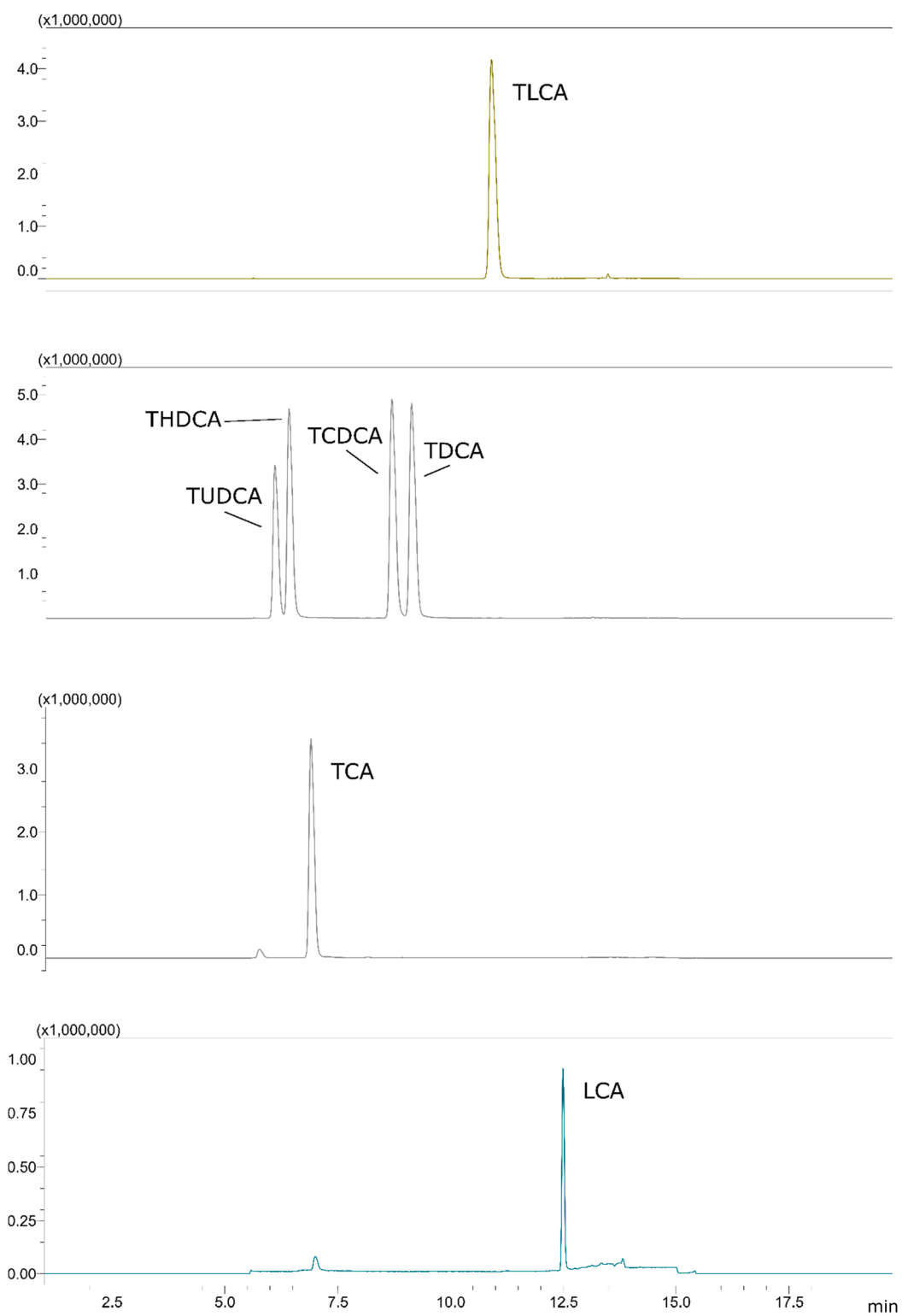


Fig. A.3. (continued).

Appendix B

See Tables B.1 and B.2.

Table B.1

MS parameters, limit of detection (LOD) and limit of quantification (LOQ) of the BAs studied.

	Mode	Q1	Q3	Retention time (min)	LOD (nM) in MeOH	LOQ (nM) in MeOH
Lithocholic acid (LCA)	SIM		375.3	12.75	10	20
Ursodeoxycholic acid (UDCA)	SIM		391.3	8.398	40	50
Hyodeoxycholic acid (HDCA)	SIM		391.3	8.889	40	50
Chenodeoxycholic acid (CDCA)	SIM		391.3	10.809	30	50
Deoxycholic acid (DCA)	SIM		391.3	11.073	5	10
Hyocholic acid (HCA)	SIM		407.3	8.145	20	30
Cholic acid (CA)	SIM		407.3	8.942	5	10
Glycolithocholic acid (GLCA)	MRM	432.3	74	11.088	5	5
Glycoursodeoxycholic acid (GUDCA)	MRM	448.3	74	6.590	5	5
Glycochenodeoxycholic acid (GCDCA)	MRM	448.3	74	9.051	5	5
Glycodeoxycholic acid (GDCA)	MRM	448.3	74	9.452	10	20
Glycocholic acid (GCA)	MRM	464.3	74	7.310	5	5
Taurolithocholic acid (TLCA)	SIM		482.3	11.077	5	10
Tauroursodeoxycholic acid (TUDCA)	SIM		498.4	6.189	5	10
Taurohyodeoxycholic acid (THDCA)	SIM		498.4	6.530	5	10
Taurochenodeoxycholic acid (TCDCA)	SIM		498.4	8.825	5	10
Taurodeoxycholic acid (TDCA)	SIM		498.4	9.283	10	20
Taurocholic acid (TCA)	SIM		514.4	7.001	5	5

SIM: Single Ion Monitoring; MRM: Multiple Reaction Monitoring; Q1: first stage MS, Q3: second stage MS; LOD: limit of detection; LOQ: limit of quantification

Table B.2

List of Primers used in RT-qPCR analysis.

Protein name	Symbol	Gene symbol	Forward primer	Reverse primer
Bile Salt Export Pump	BSEP	<i>ABCB11</i>	GTCATCTTGTGCTTCTTCCC	TCATTTGTAATCTGTCCACCA
Multidrug Resistance-associated Protein 2	MRP2	<i>ABCC2</i>	GCCCAACTGTGGCTGTGATAGG	ATCCAGGACTGCTGTGGACAT
Albumin	ALB	<i>ALB</i>	GTTCGTTACACCAAGAAAGTACC	GACCACGGATAGATAGTCTTCTG
Bile acid-CoA:amino acid N-acyltransferase	BAAT	<i>BAAAT</i>	GAGGCTGCCAATTTCTCCT	AGTACCGTGGCTGTGACTTG
Cytochrome P450 27A1	CYP27A1	<i>CYP27A1</i>	AGGCCAAGTACGGTCCAATG	GTACCAGTGGTGTCTTCCG
Cytochrome P450 3A4	CYP3A4	<i>CYP3A4</i>	TTTTGTCTTACCATAAAGGCTTT	CACAGGCTGTTGACCATCAT
Cytochrome P450 7A1	CYP7A1	<i>CYP7A1</i>	TAAGGTGTTGTGCCACGGAA	TCCATCCATCGGGTCAATGC
Hydroxymethylbilane synthase	HMBS	<i>HMBS</i>	GGCAATGCGGCTGCAA	GGGTACCCACGCGAATCAC
Hypoxanthine phosphoribosyltransferase 1	HPRT1	<i>HPRT1</i>	TATTGTAATGACCAGTCAACAG	GGTCCCTTTTACCACGCAAG
Leucine rich repeat containing G protein-coupled receptor 5	LGR5	<i>LGR5</i>	GCAGTGTTTACCTTCCC	GGTCCACACTCCAATTCTG
Farnesoid X receptor	FXR	<i>NR1H4</i>	AGGTAGCAGAGATGCCTGTAACAA	CACAGCTCATCCCTTTGATC
Ribosomal protein L19	RPL19	<i>RPL19</i>	ATGAGTATGCTCAGGCTTCAG	GATCAGCCCATCTTTGATGAG
Na ⁺ -taurocholate cotransporting polypeptide	NTCP	<i>SLC10A1</i>	GATATCACTGGTGGTTCTC	ATCATCCCTCCCTTGATGAC
Organic solute transporter- α subunit	OST α	<i>SLC51A</i>	TTGTTGCGCTCCCTATTCC	TTGTGGTCTTTCTTCCTCGGT
Organic solute transporter- β subunit	OST β	<i>SLC51B</i>	TGTGGTGGTCATTATAAGCATGG	TCTTAGGTTGTTTAGGCTGTTGTG
Organic anion transporting polypeptide 1B1	OATP1B1	<i>SLC01B1</i>	GAGCAACAGTATGGTCAGCCT	GGCAATCCAACGGTGTTC

References

- Aizarani, N., Saviano, A., Mailly, L., Durand, S., Herman, J.S., Pessaix, P., Grün, D., 2019. A human liver cell atlas reveals heterogeneity and epithelial progenitors. *Nature* 572 (7768), 199–204.
- Arnesdotter, E., Spinu, N., Firman, J., Ebbrell, D., Cronin, M.T., Vanhaecke, T., Vinken, M., 2021. Derivation, characterisation and analysis of an adverse outcome pathway network for human hepatotoxicity. *Toxicology* 459, 152856.
- Axelsson, M., Ellis, E., Mörk, B., Garmark, K., Abrahamsson, A., Björkhem, I., Einarsson, C., 2000. Bile acid synthesis in cultured human hepatocytes: support for an alternative biosynthetic pathway to cholic acid. *Hepatology* 31 (6), 1305–1312.
- Bachour-El Azzi, P., Sharanek, A., Burban, A., Li, R., Guével, R.L., Abdel-Razzak, Z., Guillouzo, A., 2015. Comparative localization and functional activity of the main hepatobiliary transporters in HepaRG cells and primary human hepatocytes. *Toxicol. Sci.* 145 (1), 157–168.
- Barter, Z.E., Bayliss, M.K., Beaune, P.H., Boobis, A.R., Carlile, D.J., Edwards, R.J., Pelkonen, O.R., 2007. Scaling factors for the extrapolation of in vivo metabolic drug clearance from in vitro data: reaching a consensus on values of human micro-somal protein and hepatocellularity per gram of liver. *Curr. Drug Metab.* 8 (1), 33–45.
- Behr, A.-C., Kwiatkowski, A., Ståhlman, M., Schmidt, F.F., Luckert, C., Braeuning, A., Buhrke, T., 2020. Impairment of bile acid metabolism by perfluorooctanoic acid (PFOA) and perfluorooctanesulfonic acid (PFOS) in human HepaRG hepatoma cells. *Arch. Toxicol.* 94 (5), 1673–1686. <https://doi.org/10.1007/s00204-020-02732-3>.
- Bell, C.C., Dankers, A.C., Lauschke, V.M., Sison-Young, R., Jenkins, R., Rowe, C., Walker, T., 2018. Comparison of hepatic 2D sandwich cultures and 3D spheroids for long-term toxicity applications: a multicenter study. *Toxicol. Sci.* 162 (2), 655–666.
- Retrieved from. (<https://www.ncbi.nlm.nih.gov/pmc/articles/PMC5888952/pdf/kfx289.pdf>)..
- Bell, C.C., Hendriks, D.F., Moro, S.M., Ellis, E., Walsh, J., Renblom, A., Snoeys, J., 2016. Characterization of primary human hepatocyte spheroids as a model system for drug-induced liver injury, liver function and disease. *Sci. Rep.* 6 (1), 1–13.
- Broutier, L., Mastrogianni, G., Versteegen, M.M., Francies, H.E., Gavarró, L.M., Bradshaw, C.R., Gaspersz, M.P., 2017. Human primary liver cancer-derived organoid cultures for disease modeling and drug screening. *Nat. Med.* 23 (12), 1424–1435. Retrieved from. (<https://www.ncbi.nlm.nih.gov/pmc/articles/PMC5722201/pdf/emss-74480.pdf>).
- Burbank, M.G., Sharanek, A., Burban, A., Mialanne, H., Aerts, H., Guguen-Guillouzo, C., Guillouzo, A., 2017. Mechanistic insights in cytotoxic and cholestatic potential of the endothelial receptor antagonists using heparg cells. *Toxicol. Sci.* 157 (2), 451–464. Retrieved from. (<https://hal-univ-rennes1.archives-ouvertes.fr/hal-01558815/document>).
- Cerec, V., Glaise, D., Garnier, D., Morosan, S., Turlin, B., Drenou, B., Corlu, A., 2007. Transdifferentiation of hepatocyte-like cells from the human hepatoma HepaRG cell line through bipotent progenitor. *Hepatology* 45 (4), 957–967.
- Chiang, J., 2013. Bile acid metabolism and signaling. *Compr. Physiol.* 3, 1191–1212 (Link). (<https://goo.gl/dC6DBB>).
- Chiang, J.Y., 2009. Bileacid metabolism and signaling in liver disease and therapy. *J. Lipid Res.* 50 (10).
- Chiang, J.Y., 2017. Bile acid metabolism and signaling in liver disease and therapy. *Liver Res.* 1 (1), 3–9. Retrieved from. (<https://www.ncbi.nlm.nih.gov/pmc/articles/PMC5663306/pdf/nihms881361.pdf>).
- Chiang, J.Y., Ferrell, J.M., 2022. Discovery of farnesoid X receptor and its role in bile acid metabolism. *Mol. Cell. Endocrinol.*, 111618

- Dawson, P.A., Lan, T., Rao, A., 2009. Bile acid transporters. *J. Lipid Res.* 50 (12), 2340–2357.
- De Bruyn, T., Chatterjee, S., Fattah, S., Keemink, J., Nicolai, J., Augustijns, P., Annaert, P., 2013. Sandwich-cultured hepatocytes: utility for in vitro exploration of hepatobiliary drug disposition and drug-induced hepatotoxicity. *Expert Opin. Drug Metab. Toxicol.* 9 (5), 589–616.
- Deferm, N., De Vocht, T., Qi, B., Van Brantegem, P., Gijbels, E., Vinken, M., Annaert, P., 2019. Current insights in the complexities underlying drug-induced cholestasis. *Crit. Rev. Toxicol.* 49 (6), 520–548. (<https://www.tandfonline.com/doi/full/10.1080/10408444.2019.1635081>).
- Ellis, E., Goodwin, B., Abrahamsson, A., Liddle, C., Mode, A., Rudling, M., Einarsson, C., 1998. Bile acid synthesis in primary cultures of rat and human hepatocytes. *Hepatology* 27 (2), 615–620. (<https://doi.org/10.1002/hep.510270241>).
- Fattinger, K., Funk, C., Pantze, M., Weber, C., Reichen, J., Stieger, B., Meier, P.J., 2001. The endothelin antagonist bosentan inhibits the canalicular bile salt export pump: a potential mechanism for hepatic adverse reactions. *Clin. Pharmacol. Ther.* 69 (4), 223–231. (<https://doi.org/10.1067/mcp.2001.114667>).
- Garzel, B., Yang, H., Zhang, L., Huang, S.-M., Polli, J.E., Wang, H., 2014. The role of bile salt export pump gene repression in drug-induced cholestatic liver toxicity. *Drug Metab. Dispos.* 42 (3), 318–322. (<https://www.ncbi.nlm.nih.gov/pmc/articles/PMC3935137/pdf/dmd.113.054189.pdf>).
- Gijbels, E., Vilas-Boas, V., Deferm, N., Devisscher, L., Jaeschke, H., Annaert, P., Vinken, M., 2019. Mechanisms and in vitro models of drug-induced cholestasis. *Arch. Toxicol.* 93 (5), 1169–1186. (<https://doi.org/10.1007/s00204-019-02437-2>).
- Gijbels, E., Vilas-Boas, V., Annaert, P., Vanhaecke, T., Devisscher, L., Vinken, M., 2020. Robustness testing and optimization of an adverse outcome pathway on cholestatic liver injury. *Arch. Toxicol.* 1–22.
- Griffin, L.M., Watkins, P.B., Perry St., C.H., Claire, R.L., Brouwer, K.L.R., 2013. Combination lopinavir and ritonavir alter exogenous and endogenous bile acid disposition in sandwich-cultured rat hepatocytes. *Drug Metab. Dispos.* 41 (1), 188. (<https://doi.org/10.1124/dmd.112.047225>).
- Guguen-Guillouzo, C., Guillouzo, A., 2019. Setup and use of HepaRG cells in cholestasis research. In: Vinken, M. (Ed.), *Experimental Cholestasis Research*. Springer New York, New York, NY, pp. 291–312.
- Hendriks, D.F., Fredriksson Puigvert, L., Messner, S., Mortiz, W., Ingelman-Sundberg, M., 2016. Hepatic 3D spheroid models for the detection and study of compounds with cholestatic liability. *Sci. Rep.* 6, 35434. (<https://doi.org/10.1038/srep35434>).
- Hengstler, J.G., Utesch, D., Steinberg, P., Platt, K., Diener, B., Ringel, M., Gerl, M., 2000. Cryopreserved primary hepatocytes as a constantly available in vitro model for the evaluation of human and animal drug metabolism and enzyme induction. *Drug Metab. Rev.* 32 (1), 81–118.
- Huch, M., Gehart, H., Van Boxtel, R., Hamer, K., Blokzijl, F., Versteegen, M.M., de Ligt, J., 2015. Long-term culture of genome-stable bipotent stem cells from adult human liver. *Cell* 160 (1–2), 299–312. Retrieved from.
- Jia, W., Xie, G., Jia, W., 2018. Bile acid-microbiota crosstalk in gastrointestinal inflammation and carcinogenesis. *Nat. Rev. Gastroenterol. Hepatol.* 15 (2), 111–128. (<https://doi.org/10.1038/nrgastro.2017.119>).
- Kanebratt, K.P., Andersson, T.B., 2008. Evaluation of HepaRG cells as an in vitro model for human drug metabolism studies. *Drug Metab. Dispos.* 36 (7), 1444–1452. (<https://dmd.aspetjournals.org/content/36/7/1444.long>).
- Laverty, H.G., Antoine, D.J., Benson, C., Chaponda, M., Williams, D., Park, B.K., 2010. The potential of cytokines as safety biomarkers for drug-induced liver injury. *Eur. J. Clin. Pharmacol.* 66 (10), 961–976.
- LeCluyse, E.L., Alexandre, E., 2010. Isolation and culture of primary hepatocytes from resected human liver tissue. *Hepatocytes*. Springer, pp. 57–82.
- Lepist, E.-I., Gillies, H., Smith, W., Hao, J., Hubert St., C., Claire III, R.L., Ray, A.S., 2014. Evaluation of the endothelin receptor antagonists ambrisentan, bosentan, macitentan, and sitaxsentan as hepatobiliary transporter inhibitors and substrates in sandwich-cultured human hepatocytes. *PLOS ONE* 9 (1), e87548. Retrieved from. (<https://www.ncbi.nlm.nih.gov/pmc/articles/PMC3907537/pdf/pone.0087548.pdf>).
- Lu, S., Zhang, J., Lin, S., Zheng, D., Shen, Y., Qin, J., Wang, S., 2021. Recent advances in the development of in vitro liver models for hepatotoxicity testing. *Bio-Des. Manuf.* 4 (4), 717–734.
- Marsee, A., Roos, F.J., Versteegen, M.M., Roos, F., Versteegen, M., Clevers, H., Peng, W.C., 2021. Building consensus on definition and nomenclature of hepatic, pancreatic, and biliary organoids. *Cell Stem Cell* 28 (5), 816–832.
- Messner, S., Fredriksson, L., Lauschke, V.M., Roessger, K., Escher, C., Bober, M., Moritz, W., 2018. Transcriptomic, proteomic, and functional long-term characterization of multicellular three-dimensional human liver microtissues. *Appl. Vitro. Toxicol.* 4 (1), 1–12.
- Nguyen, L., Jager, M., Lieshout, R., de Ruiter, P.E., Locati, M.D., Besselink, N., de Jonge, J., 2021. Precancerous liver diseases do not cause increased mutagenesis in liver stem cells. *Commun. Biol.* 4 (1), 1–9.
- Noor, F., 2015. A shift in paradigm towards human biology-based systems for cholestatic-liver diseases. *J. Physiol.* 593 (23), 5043–5055. (<https://doi.org/10.1113/JP271124>).
- Olson, H., Betton, G., Robinson, D., Thomas, K., Monro, A., Kolaja, G., Bracken, W., 2000. Concordance of the toxicity of pharmaceuticals in humans and in animals. *Regul. Toxicol. Pharmacol.* 32 (1), 56–67.
- Oorts, M., Van Brantegem, P., Deferm, N., Chatterjee, S., Dreesen, E., Cooreman, A., Annaert, P., 2021. Bosentan alters endo-and exogenous bile salt disposition in sandwich-cultured human hepatocytes. *J. Pharmacol. Exp. Ther.* 379 (1), 20–32.
- Prior, N., Inacio, P., Huch, M., 2019. Liver organoids: from basic research to therapeutic applications. *Gut* 68 (12), 2228–2237. Retrieved from. (<https://gut.bmj.com/content/gutjnl/68/12/2228.full.pdf>).
- R Core Team, 2020. R: A language and environment for statistical computing. Vienna, Austria: R Foundation for Statistical Computing. Retrieved from (<https://www.R-project.org/>).
- Ramli, M.N.B., Lim, Y.S., Koe, C.T., Demircioglu, D., Tng, W., Gonzales, K.A.U., Soe, E.L., 2020. Human pluripotent stem cell-derived organoids as models of liver disease. *Gastroenterology* 159 (4), 1471–1486 e1412. ([https://www.gastrojournal.org/article/S0016-5085\(20\)34762-4/pdf](https://www.gastrojournal.org/article/S0016-5085(20)34762-4/pdf)).
- Reza, H.A., Okabe, R., Takebe, T., 2021. Organoid transplant approaches for the liver. *Transpl. Int.* 34 (11), 2031–2045.
- Rodrigues, Lai, Y., Cvijic, M.E., Elkin, L.L., Zvyaga, T., Soars, M.G., 2014. Drug-induced perturbations of the bile acid pool, cholestasis, and hepatotoxicity: mechanistic considerations beyond the direct inhibition of the bile salt export pump. *Drug Metab. Dispos.* 42 (4), 566. (<https://doi.org/10.1124/dmd.113.054205>).
- Russell, D.W., 2003. The enzymes, regulation, and genetics of bile acid synthesis. *Annu. Rev. Biochem.* 72 (1), 137–174.
- Schneeberger, K., Sánchez-Romero, N., Ye, S., van Steenbeek, F.G., Oosterhoff, L.A., Pla Palacin, I., Spee, B., 2020. Large-scale production of LGR5-positive bipotential human liver stem cells. *Hepatology*. (<https://doi.org/10.1002/hep.31037>).
- Sharanek, A., Burban, A., Humbert, L., Bachour-El Azzi, P., Felix-Gomes, N., Rainteau, D., Guillouzo, A., 2015. Cellular accumulation and toxic effects of bile acids in cyclosporine a-treated heparG hepatocytes. *Toxicol. Sci.* 147 (2), 573–587. (<https://doi.org/10.1093/toxsci/kfv155>).
- Sohlenius-Sternbeck, A.-K., 2006. Determination of the hepatocellularity number for human, dog, rabbit, rat and mouse livers from protein concentration measurements. *Toxicol. Vitro* 20 (8), 1582–1586.
- Starokozhko, V., Greupink, R., van de Broek, P., Soliman, N., Ghimire, S., de Graaf, I.A. M., Groothuis, G.M.M., 2017. Rat precision-cut liver slices predict drug-induced cholestatic injury. *Arch. Toxicol.* 91 (10), 3403–3413. (<https://doi.org/10.1007/s00204-017-1960-7>).
- Susukida, T., Sekine, S., Nozaki, M., Tokizono, M., Ito, K., 2015. Prediction of the clinical risk of drug-induced cholestatic liver injury using an in vitro sandwich cultured hepatocyte assay. *Drug Metab. Dispos.* 43 (11), 1760–1768. Retrieved from. (<https://dmd.aspetjournals.org/content/43/11/1760.long>).
- Susukida, T., Sekine, S., Nozaki, M., Tokizono, M., Oizumi, K., Horie, T., Ito, K., 2016. Establishment of a drug-induced, bile acid-dependent hepatotoxicity model using HepaRG cells. *J. Pharm. Sci.* 105 (4), 1550–1560. Retrieved from. (<https://www.sciencedirect.com/science/article/pii/S0022354916003099?via%3Dihub>).
- van Tonder, J.J., Steenkamp, V., Gulumian, M., 2013. Pre-clinical assessment of the potential intrinsic hepatotoxicity of candidate drugs. *New Insights into Toxicity and Drug Testing*. IntechOpen.
- Versteegen, M.M., Roos, F.J., Burka, K., Gehart, H., Jager, M., de Wolf, M., van Huizen, N. A., 2020. Human extrahepatic and intrahepatic cholangiocyte organoids show region-specific differentiation potential and model cystic fibrosis-related bile duct disease. *Sci. Rep.* 10 (1), 1–16.
- Vilas-Boas, V., Gijbels, E., Cooreman, A., Van Campenhout, R., Gustafson, E., Leroy, K., Vinken, M., 2019. Industrial, biocide, and cosmetic chemical inducers of cholestasis. *Chem. Res. Toxicol.* 32 (7), 1327–1334. Retrieved from. (<https://www.ncbi.nlm.nih.gov/pmc/articles/PMC7176485/pdf/EMS86148.pdf>).
- Vilas-Boas, V., Gijbels, E., Jonckheer, J., De Waele, E., Vinken, M., 2020. Cholestatic liver injury induced by food additives, dietary supplements and parenteral nutrition. *Environ. Int.* 136, 105422. (<https://doi.org/10.1016/j.envint.2019.105422>).
- Vinken, M., 2018. In vitro prediction of drug-induced cholestatic liver injury: a challenge for the toxicologist. *Arch. Toxicol.* 92 (5), 1909–1912. Retrieved from.
- Vorink, S.U., Zhou, Y., Ingelman-Sundberg, M., Lauschke, V.M., 2018. Prediction of drug-induced hepatotoxicity using long-term stable primary hepatic 3D spheroid cultures in chemically defined conditions. *Toxicol. Sci.* 163 (2), 655–665.
- Wickham, R., 2019. tidyverse: Easily Install and Load the 'Tidyverse'. R package (Version version 1.3.0). Retrieved from (<https://CRAN.R-project.org/package=tidyverse>).
- Yang, Q., Li, A.P., 2021. Messenger RNA expression of albumin, transferrin, transthyretin, asialoglycoprotein receptor, cytochrome P450 isoform, uptake transporter, and efflux transporter genes as a function of culture duration in prolonged cultured cryopreserved human hepatocytes as collagen-matrigel sandwich cultures: evidence for redifferentiation upon prolonged culturing. *Drug Metab. Dispos.* 49 (9), 790–802.